
Exact Information Bottleneck with Invertible Neural Networks: Getting the Best of Discriminative and Generative Modeling

Lynton Ardizzone^{*1}, Radek Mackowiak^{*2}, Carsten Rother¹, Ullrich Köthe¹

¹ Visual Learning Lab, Heidelberg University, Heidelberg, Germany,

² Robert Bosch Corporate Research - Computer Vision, Hildesheim, Germany

* These authors contributed equally to this work

Abstract

Generative models are more informative about underlying phenomena than discriminative ones and offer superior uncertainty quantification and out-of-distribution robustness. However, these advantages often come at the expense of reduced classification accuracy. The Information Bottleneck objective (IB) formulates this trade-off in a clean information-theoretic way, but its practical application is hampered by a lack of accurate high-dimensional estimators of mutual information (MI), its main constituent. To overcome this limitation, we develop the theory and methodology of IB-INNs, which optimize the IB objective by means of Invertible Neural Networks (INNs), without the need for approximations of MI. Our experiments show that IB-INNs allow for a precise adjustment of the generative/discriminative trade-off: They learn accurate models of the class conditional likelihoods, generalize well to unseen data and reliably detect out-of-distribution examples, while at the same time exhibiting classification accuracy close to purely discriminative feed-forward networks.

Code available at github.com/VLL-HD/FrEIA

1 INTRODUCTION

The distinction between discriminative and generative classifiers (DCs vs. GCs) is fundamental to machine learning. DCs directly predict posterior class probabilities $p(Y|X)$, where X and Y denote input and output variables respectively. GCs instead model the joint probability $p(X, Y)$, usually as a product of class priors $p(Y)$ and conditional data likelihoods $p(X|Y)$.

They are able to generate synthetic data, and posterior class probabilities can simply be inferred by Bayes' rule $p(Y|X) = p(X|Y)p(Y)/\mathbb{E}_{p(Y)} [p(X|Y)]$.

DCs optimize prediction performance directly and therefore achieve better results in this respect. However, their models for $p(Y|X)$ tend to be most accurate near decision boundaries (where it matters), but deteriorate away from them (where deviations incur no noticeable loss). Consequently, they are poorly calibrated (Guo et al., 2017) and out-of-distribution data can not be recognized at test time (Ovadia et al., 2019). In contrast, GCs model full likelihoods $p(X|Y)$ and thus implicitly full posteriors $p(Y|X)$, which leads to the opposite behavior – better predictive uncertainty at the price of reduced accuracy.

In practice, models trained in a purely generative way (in particular with maximum likelihood), achieve highly unsatisfactory accuracy, so that some recent work has called into question the overall effectiveness of GCs (Fetaya et al., 2019; Nalisnick et al., 2019b). Others have introduced different architectures and augmented losses (Jacobsen et al., 2019; Nalisnick et al., 2019a), that lead to an improvement of the discriminative capabilities. In-depth studies of the ideal cases (Bishop & Lasserre, 2007; Bishop, 2007) revealed the existence of a trade-off, controlling the balance between discriminative and generative performance. The existence of a trade-off is not self evident, as in principle, a more accurate generative model should also lead to better classification.

We propose the Information Bottleneck (IB) objective (Tishby et al., 2000) as an alternative viewpoint of this phenomenon, when applied to generative classification. IB formulates the discriminative/generative trade-off in a very general information-theoretic form: It postulates existence of a latent space Z , where all information flow between X and Y is channeled through (hence the method's name). In order to optimize pre-

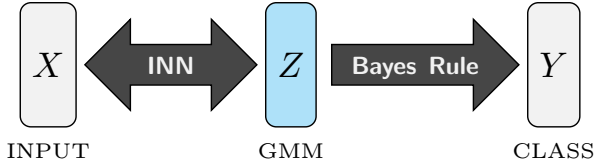


Figure 1: Our generative classifier as the Information Bottleneck Invertible Neural Network (IB-INN).

dictive performance, IB attempts to maximize the mutual information $I(Y, Z)$ between Y and Z . Jointly, it strives to minimize the mutual information $I(X, Z)$ between X and Z , forcing the model to ignore irrelevant aspects of X , which do not contribute to classification performance and only increase the potential for overfitting. The objective can therefore be expressed as

$$\mathcal{L}_{\text{IB}} = I(X, Z) - \beta I(Y, Z). \quad (1)$$

Unfortunately, practical application of IB as a loss function is difficult because existing estimators for mutual information (MI) are not sufficiently reliable in high dimensions. The Variational Information Bottleneck (VIB, Alemi et al., 2017; Kolchinsky et al., 2017) provides a feasible approximation in form of an upper bound for IB, which however does not work as well as the asymptotically exact solution presented in this work.

Using Invertible Neural Networks (INNs), we can, for the first time, train generative classifiers directly with the IB objective, cf. Fig. 1. This major advance arises from two critical properties of this network type: (i) the transformation between X and Z has a tractable Jacobian determinant, and (ii) the latent space Z can be shaped as a Gaussian Mixture Model (GMM). As a result, the IB objective is analytically expressible in terms of the change-of-variables formula, allowing for standard gradient descent training without additional approximations. Moreover, properties (i) and (ii) facilitate latent space exploration which enables out-of-distribution detection and the analysis of class similarities. The trade-off parameter β occurring in the IB loss (1) allows us to explicitly alter the trade-off between our model’s classification performance and its generative modeling capabilities. When β is adjusted properly, our experiments reveal that IB-INNs simultaneously exhibit high predictive accuracy, well calibrated uncertainties and allow to reliably detect out-of-distribution examples.

To summarize, we combine two concepts – the Information Bottleneck (IB) objective and Invertible Neural Networks (INNs) – into a new generative classifier type called IB-INN. Our contributions are as follows:

- We derive an asymptotically exact formulation of the IB loss for a special GC type by utilizing INNs.
- We show experimentally that our models out-

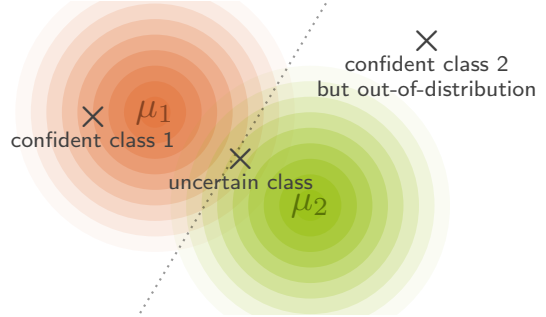


Figure 2: Illustration of the latent output space of a generative classifier. The two class likelihoods for $Y = \{1, 2\}$ are parameterized by their means $\mu_{\{1,2\}}$. The dotted line represents the decision boundary between the two classes. A confident, an uncertain, and an out-of-distribution sample is illustrated.

perform existing GCs on CIFAR10/100 in terms of classification error, and incur at worst minor degradation relative to feed-forward DCs.

- We demonstrate good uncertainty quantification in terms of accurate posterior calibration and reliable outlier detection.

2 METHOD

In the following, upper case letters denote random variables (RVs) (e.g. X) and lower case letters their instances (e.g. x). The probability density function of an RV is written as $p(X)$, the evaluated density as $p(x)$ (or $p(X = x)$ when ambiguous), and all RVs are understood as vector quantities. We distinguish true distributions from modeled ones by the letters p and q respectively. The distributions q always depend on model parameters, but we do not make this explicit to avoid notation clutter. The proofs to all Propositions are provided in the appendix.

Our models have two kinds of learnable parameters:

1. An invertible neural network with parameters θ bijectively maps inputs X to latent variables Z

$$\text{INN: } Z = g_{\theta}(X) \Leftrightarrow X = g_{\theta}^{-1}(Z) \quad (2)$$

2. A Gaussian mixture model with means μ_y and unit covariance matrices is used as a reference distribution for the latents Z

$$q(Z | Y) = \mathcal{N}(\mu_y, \mathbb{I}) \quad (3)$$

$$q(Z) = \sum_y p(y) \mathcal{N}(\mu_y, \mathbb{I}) \quad (4)$$

where y are the class labels. For simplicity, we assume that the label distribution is known, i.e. $q(Y) = p(Y)$.

Our derivation rests on a quantity we call *mutual cross-information* in analogy to the well-known cross-entropy

$$CI(U, V) = \mathbb{E}_{u, v \sim p(U, V)} \left[\log \frac{q(u, v)}{q(u)q(v)} \right] \quad (5)$$

Note that the expectation is taken over the true distribution, whereas the logarithm involves model distributions. The following proposition (proof in Appendix) clarifies the relationship between mutual information I and CI :

Proposition 1. *Assume that $q(\cdot)$ can be chosen from a sufficiently rich model family (e.g. a universal density estimator). Then for every $\eta > 0$ there is a model such that*

$$|I(U, V) - CI(U, V)| < \eta \quad (6)$$

and $I(U, V) = CI(U, V)$ if $p(u, v) = q(u, v)$.

2.1 Estimating Mutual Information with INNs

Estimation of the mutual cross-information $CI(X, Z)$ between inputs and latents is problematic for deterministic mappings from X to Z (Amjad & Geiger, 2018), and specifically for invertible networks, which are bijective by construction. In this case, the joint distributions $q(X, Z)$ and $p(X, Z)$ are not valid Radon-Nikodym densities and both CI and I are therefore undefined. We resolve this degeneracy by means of data augmentation: Instead of inputting X to the network, we feed it with a noisy version $X' = X + \mathcal{E}$, where $\mathcal{E} \sim \mathcal{N}(0, \sigma^2 \mathbb{I}) = p(\mathcal{E})$ is Gaussian with mean zero and covariance $\sigma^2 \mathbb{I}$. This is motivated by practical experience: For normalizing flows and similar models, such noise augmentation is required anyway to dequantize X (i.e. to turn discrete pixel values into real numbers). In other words, the INN actually learns the mapping $Z_{\mathcal{E}} = g_{\theta}(X + \mathcal{E})$, which guarantees that $CI(X, Z_{\mathcal{E}})$ is well-defined. Minimizing $CI(X, Z_{\mathcal{E}})$ according to the IB principle means that $g_{\theta}(X + \mathcal{E})$ is encouraged to amplify the noise \mathcal{E} and ignore the data X , see Fig. 3. If the global minimum can be reached, I and CI will coincide, as $CI(X, Z_{\mathcal{E}})$ is an upper bound (cf. Prop. 1):

Proposition 2. *For the specific case that $Z_{\mathcal{E}} = g_{\theta}(X + \mathcal{E})$, it holds that $I(X, Z_{\mathcal{E}}) \leq CI(X, Z_{\mathcal{E}})$.*

We now derive the training procedure for flow-type networks with the noise-augmented $CI(X, Z_{\mathcal{E}})$ in the limit of small noise $\sigma \rightarrow 0$. Full details found in appendix. We decompose the mutual cross-information into two terms

$$CI(X, Z_{\mathcal{E}}) = \mathbb{E}_{x, \varepsilon \sim p(X), p(\varepsilon)} \left[-\log q(Z_{\mathcal{E}} = g_{\theta}(x + \varepsilon)) \right] + \underbrace{\mathbb{E}_{x, \varepsilon \sim p(X), p(\varepsilon)} \left[\log q(Z_{\mathcal{E}} = g_{\theta}(x + \varepsilon) \mid X = x) \right]}_{:=C}$$

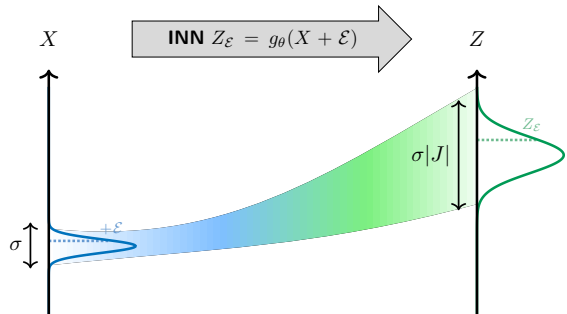


Figure 3: The more the noise is amplified in relation to the noise-free input, the lower the mutual cross-information between noisy latent vector $Z_{\mathcal{E}}$ and noise-free input X .

The first expectation can be approximated by the empirical mean over a finite dataset, because the Gaussian mixture distribution $q(Z_{\mathcal{E}})$ is known analytically. To approximate the second term, we first note that the condition $X = x$ can be replaced with $Z = g_{\theta}(x)$, because g_{θ} is bijective and both conditions convey the same information

$$C = \mathbb{E}_{p(X), p(\varepsilon)} \left[\log q(Z_{\mathcal{E}} = g_{\theta}(x + \varepsilon) \mid Z = g_{\theta}(x)) \right]$$

We now linearize g_{θ} by its first order Taylor expansion

$$g_{\theta}(x + \varepsilon) = g_{\theta}(x) + J_x \varepsilon + O(\sigma^2)$$

where $J_x = \frac{\partial g_{\theta}(X)}{\partial X} \Big|_x$ denotes the Jacobian at $X = x$. Inserting this into C , the $O(\sigma^2)$ can be moved out of the expectation due to the dominated convergence theorem (DCT):

$$C = \mathbb{E}_{p(X), p(\varepsilon)} \left[\log q(g_{\theta}(x) + J_x \varepsilon \mid g_{\theta}(x)) \right] + O(\sigma^2)$$

Since ε is Gaussian with mean zero and covariance $\sigma^2 \mathbb{I}$, the conditional distribution is Gaussian with mean $g_{\theta}(x)$ and covariance $\sigma^2 J_x J_x^T$. The expectation with respect to $p(\varepsilon)$ is thus the negative entropy of a multivariate Gaussian and can be computed analytically as well

$$\begin{aligned} C &= \mathbb{E}_{p(X)} \left[-\frac{1}{2} \log (\det(2\pi e \sigma^2 J_x J_x^T)) \right] + O(\sigma^2) \\ &= \mathbb{E}_{p(X)} \left[-\log |\det(J_x)| \right] \\ &\quad - d \log(\sigma) - \frac{d}{2} \log(2\pi e) + O(\sigma^2) \end{aligned}$$

with d the dimension of X . To avoid running the model twice (for x and $x + \varepsilon$), we approximate the expectation of the Jacobian determinant by 0th-order Taylor expansion as

$$\mathbb{E}_{p(X)} [\log |\det(J_x)|] = \mathbb{E}_{p(X), p(\varepsilon)} [\log |\det(J_{\varepsilon})|] + O(\sigma)$$

where J_ε is the Jacobian evaluated at $x+\varepsilon$ instead of x . The residual can be moved outside of the expectation because of DCT, and because J_ε is always bounded in our networks.

Putting everything together, we drop terms from $CI(X, Z_\varepsilon)$ that are independent of the model or vanish with rate at least $O(\sigma)$ as $\sigma \rightarrow 0$. The resulting loss \mathcal{L}_X becomes

$$\mathcal{L}_X = \mathbb{E}_{p(X), p(\varepsilon)} \left[-\log q(g_\theta(x+\varepsilon)) - \log |\det(J_\varepsilon)| \right] \quad (7)$$

Since the network’s generative distribution is defined by the change of variables formula as

$$q_X(x) = q(Z = g_\theta(x)) |\det(J_x)|, \quad (8)$$

we recognize \mathcal{L}_X as the negative log-likelihood of the perturbed data under q_X

$$\mathcal{L}_X = \mathbb{E}_{p(X), p(\varepsilon)} \left[-\log q_X(x + \varepsilon) \right] \quad (9)$$

The crucial difference between $CI(X, Z_\varepsilon)$ and \mathcal{L}_X is the elimination of the term $-d \log(\sigma)$. It is huge for small σ and would dominate the model-dependent terms, making minimization of $CI(X, Z_\varepsilon)$ very hard. Intuitively, $CI(X, Z_\varepsilon)$ diverging for $\sigma \rightarrow 0$ highlights why $CI(X, Z)$ is undefined. In practice, we estimate \mathcal{L}_X by the empirical mean $\mathcal{L}_X^{(N)}$ on a training set $\{x_i, \varepsilon_i\}_{i=1}^N$ of size N :

$$\mathcal{L}_X^{(N)} = \frac{1}{N} \sum_{i=1}^N \left[-\log q(g_\theta(x_i + \varepsilon_i)) - \log |\det(J_i)| \right] \quad (10)$$

where J_i is the Jacobian of g_θ evaluated at $x_i + \varepsilon_i$.

It remains to be shown that replacing $I(X, Z_\varepsilon)$ with $\mathcal{L}_X^{(N)}$ in the IB loss Eq. 1 does not fundamentally change the solution of the learning problem in the limit of large N , small σ and sufficient model power. Sufficient model power here means that the family of generative distributions realizable by g_θ should be a universal density estimator. This is the case if g_θ can represent increasing triangular maps (Bogachev et al., 2005), which has been proven for certain network architectures explicitly (e.g. Jaini et al., 2019; Huang et al., 2018). Propositions 1 & 2 then tell us that we may optimize $CI(X, Z_\varepsilon)$ as an estimator of $I(X, Z_\varepsilon)$. The above derivation of the loss can be strengthened into

Proposition 3. *For any $\epsilon, \eta > 0$ and $0 < \delta < 1$ there are $\sigma_0 > 0$ and $N_0 \in \mathbb{N}$, such that $\forall N \geq N_0$ and $\forall \sigma < \sigma_0$,*

$$\Pr \left(\left| CI(X, Z_\varepsilon) + d \log \sqrt{2\pi e \sigma^2} - \mathcal{L}_X^{(N)} \right| < \epsilon \right) > 1 - \delta$$

and

$$\Pr \left(\left\| \frac{\partial}{\partial \theta} CI(X, Z_\varepsilon) - \frac{\partial}{\partial \theta} \mathcal{L}_X^{(N)} \right\| < \eta \right) > 1 - \delta$$

holds uniformly for all model parameters θ .

The first statement proves consistence of $\mathcal{L}_X^{(N)}$, and the second justifies gradient-descent optimization on the basis of $\mathcal{L}_X^{(N)}$. Proofs can be found in the appendix.

2.2 The IB-INN

Similarly to the first term in the IB-loss in Eq. 1, we also replace the mutual information $I(Y, Z)$ with

$$\begin{aligned} CI(Y, Z_\varepsilon) &= \mathbb{E}_{x, y \sim p(X, Y), \varepsilon \sim p(\varepsilon)} \left[\log \frac{q(Z_\varepsilon = g_\theta(x + \varepsilon), y)}{q(Z_\varepsilon = g_\theta(x + \varepsilon)) p(y)} \right] \end{aligned}$$

Inserting the likelihood $q(z|y) = \mathcal{N}(z; \mu_y, \mathbb{I})$ of our latent Gaussian mixture model and recalling that $q(Y) = p(Y)$, this can be decomposed into

$$\begin{aligned} CI(Y, Z_\varepsilon) &= \mathbb{E}_{y \sim p(Y)} [-\log p(y)] \quad (11) \\ &+ \mathbb{E}_{x, y \sim p(X, Y), \varepsilon \sim p(\varepsilon)} \left[\log \frac{q(g_\theta(x + \varepsilon) | y) p(y)}{\sum_{y'} q(g_\theta(x + \varepsilon) | y') p(y')} \right] \end{aligned}$$

The first expectation is independent of the model and can be dropped, whereas the second is the expectation of the GMM’s log-posterior $\log q(y|z)$. Since all mixture components have unit covariance, the elements of Z are conditionally independent and the likelihood factorizes as $q(z|y) = \prod_j q(z_j|y)$, so that $q(y|z)$ can be interpreted as a naive Bayes classifier. In contrast to a naive Bayes classifier in data space, which typically performs badly because raw features are not conditionally independent, our training process pushes latent features towards conditional independence and results in very accurate classification.

Defining the loss $\mathcal{L}_Y^{(N)}$ as the empirical mean of the log-posterior in a training set $\{x_i, y_i, \varepsilon_i\}_{i=1}^N$ of size N , we get

$$\mathcal{L}_Y^{(N)} = \frac{1}{N} \sum_{i=1}^N \log \frac{\mathcal{N}(g_\theta(x_i + \varepsilon_i); \mu_{y_i}, \mathbb{I}) p(y_i)}{\sum_{y'} \mathcal{N}(g_\theta(x_i + \varepsilon_i); \mu_{y'}, \mathbb{I}) p(y')} \quad (12)$$

and our model parameters θ and $\{\mu_1, \dots, \mu_K\}$ are trained by gradient descent of the IB-INN loss

$$\mathcal{L}_{\text{IB-INN}}^{(N)} = \mathcal{L}_X^{(N)} - \beta \mathcal{L}_Y^{(N)} \quad (13)$$

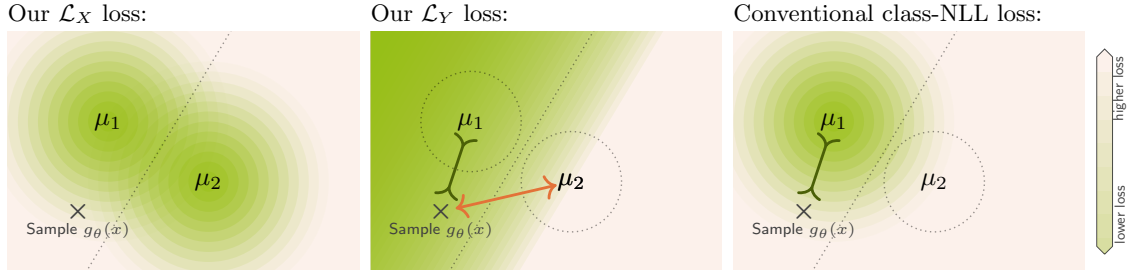


Figure 4: Illustration of the loss landscape for our IB formulation (*left, middle*) and standard class-conditional negative-log-likelihood (*right*). The loss is shown for an input x belonging to class $Y = 1$, green areas correspond to low loss. The green and orange arrows indicate attractive and repulsive interactions with the cluster centers.

2.3 Advantages of the IB-Loss

In this section we will interpret and discuss the nature of the loss function in Eq. 13. We also form an intuitive understanding of why it is more suitable than the class-conditional negative-log-likelihood (‘class-NLL’) traditionally used for generative classifiers of this type. The findings are represented graphically in Fig. 4.

\mathcal{L}_X -term: As demonstrated in Eq. 9, the term is the (unconditional) negative-log-likelihood loss used for normalizing flows, with the difference that $q(Z)$ is a GMM rather than a unimodal Gaussian. We conclude that this loss term encourages the INN to become an accurate likelihood model under the marginalized latent distribution and completely ignores any class content.

\mathcal{L}_Y -term: Examining Eq. 12, we see that for any pair $g(x + \varepsilon), y$, the cluster centers ($\mu_{Y \neq y}$) of the other classes are repulsed, while $g_\theta(x + \varepsilon)$ and the correct cluster center μ_y are drawn together. Note that the class-NLL loss only captures the second aspect, and therefore has a much weaker training signal. We can also view this in a different way: by substituting $q(x|y) |\det(J_\theta(x))|^{-1}$ for $q(z|y)$ the second summand of Eq. 11 simplifies to $\log q(y|x)$, since the Jacobian cancels out. This means that the \mathcal{L}_Y loss directly maximizes the correct class probability, while ignoring the data likelihood. Again, this improves the training signal, as Fetaya et al. (2019) showed that the data likelihood dominates the class-NLL loss, so that the discriminative aspect is not properly learned.

Classical class-NLL loss: For $\beta = 1$, the IB-INN loss reduces to the class-NLL loss, because the first summand in Eq. 10 cancels with the denominator in Eq. 12. The INN is then no longer penalized for overlapping mixture components, and the GMM loses its class discriminatory nature, as Fig. 4 illustrates. This is explained in more detail by Fetaya et al. (2019), who show that indeed the class-NLL loss causes a vanishingly small training signal for the class separation: points are only drawn towards the correct class, but there is no term repulsing them from the incorrect classes. For an unregularized model trained with

class-NLL, this causes all cluster centers to collapse together, leading the INN to effectively just model the marginal data likelihood.

2.4 Practical Implementation

We learn μ_Y as a free parameter jointly with the remaining model parameters in an end-to-end fashion using the loss in Eq. 13. The entire training is performed in log-space for numerical stability, as the likelihoods become both too large and too small otherwise (see Appendix Sec. 2 for details). We apply two additional techniques while learning the model, label smoothing and loss rebalancing:

Label smoothing We observed that the individual class means μ_Y drift apart during training, because training with hard labels enforces the Gaussian mixture components to become perfectly separated. This can cause problems during training, as there is a high loss barrier between the clusters due to \mathcal{L}_X , preventing points from moving smoothly from one class to the other during training. To avoid this effect, we simply apply a small amount of label smoothing (Szegedy et al., 2016), where the one-hot training vectors are softened with $\alpha = 0.05$ in our case. We do the same for all comparison models.

Loss rebalancing To avoid the laborious process of having to adjust hyperparameters for vastly different loss magnitudes, we employ the following rebalancing scheme: Firstly, we divide the loss \mathcal{L}_X by the number of dimensions of X . This ensures that \mathcal{L}_X remains in a similar range when changing e.g. the input image size, as it scales linearly with the number of input dimensions. Secondly, we define a matching $\tilde{\beta} \equiv \beta / \dim(X)$. Lastly, we reweight the entire loss by a factor $2 / (1 + \tilde{\beta})$. This ensures that the loss keeps the same magnitude when changing $\tilde{\beta}$ over wide ranges. Thanks to this rebalancing scheme, we can use the same learning rate and hyperparameters for all experiments:

$$\mathcal{L}_{\text{IB}}^{(N)} = \frac{2}{1 + \tilde{\beta}} \left(\frac{\mathcal{L}_X^{(N)}}{\dim(X)} - \tilde{\beta} \mathcal{L}_Y^{(N)} \right) \quad (14)$$

3 EXPERIMENTS

We construct our IB-INN by combining the design efforts of various previous works on INNs and normalizing flows. In brief, we use a Real-NVP design consisting of affine coupling blocks (Dinh et al., 2017), with added improvements from recent works, such as Kingma & Dhariwal (2018); Jacobsen et al. (2019, 2018); Ardizzone et al. (2019). A more detailed description of the architecture is provided in the appendix.

3.1 Comparison of Methods

In addition to the IB-INN, we train several alternative methods. For each, we use exactly the same INN model, or an equivalent feed-forward ResNet model. Every method has the exact same hyperparameters and training procedure, the only difference being the loss function, and the lack of invertibility for pure feed-forward models.

Feed-forward As a baseline, we train a feed-forward ResNet (He et al., 2016) with softmax cross entropy loss. Each affine coupling is simply replaced by a ResNet block. Except for the invertibility, the architectures are identical.

i-RevNet (Jacobsen et al., 2018): To rule out any differences stemming from the constraint of invertibility, we additionally train the INN as a standard softmax classifier, by projecting the outputs to class logits. While the architecture is invertible, the model is not generative and trained as a standard feed-forward classifier.

Variational Information Bottleneck (VIB): We train the VIB, as presented by Alemi et al. (2017), using a feed-forward ResNet. Note that the authors define their β in the opposite way, by weighting $I(X, Z)$. For consistency we convert this to our definition of β .

Class-NLL: As a standard generative classifier, we firstly train an INN with a GMM in latent space completely naively as a conditional generative model, using the class-conditional maximum likelihood loss $\mathcal{L}_{\text{class-NLL}} = -\mathbb{E} \log(q_\theta(x|y))$. Secondly, we also train a regularized version, to increase the classification accuracy. The regularization consists of constraining the class centroids μ_Y to points on a sphere with a fixed radius. As the radius becomes comparable to the typical intra-class distances, the training signal for the classification is amplified. We therefore choose $\sqrt{\dim(Z)}$ as radius.

3.2 Quantitative measurements

In the following, we describe the scores reported in Tab. 1.

Calibration error: In general, the calibration curve measures whether the confidence of a model agrees with its actual performance. All prediction outputs

are binned according to their predicted probability P ('confidence'), and it is recorded which fraction of predictions in each bin was correct, Q . For a perfectly calibrated model, we have $P = Q$, e.g. predictions with 30% confidence are correct 30% of the time. There are various metrics to measure deviation from this perfect behaviour, and we largely adhere to those used by Guo et al. (2017). Exact descriptions found in Appendix. Specifically, we consider the expected calibration error (ECE), the maximum calibration error (MCE), and a quantity termed the overconfidence (OVC). The overconfidence measures the normalized fraction of highly confident but wrong predictions. It should be $\in [0, 1]$ for a well calibrated model, and is $\gg 1$ for an overconfident one. Because we find the metrics to be partly inconsistent, we also include the geometric mean of all three (i.e. $\sqrt[3]{\text{ECE} \cdot \text{MCE} \cdot \max(1, \text{OVC})}$). The geometric mean is used because it properly accounts for the different magnitudes of the metrics. Note, that we only penalize the OVC if it is above the upper bound for a well-calibrated model.

Out-of-distribution (OoD) prediction entropy: For data that is OoD, we expect from a model that it returns uncertain class predictions, as it has not been trained on such data. In the ideal case, each class is assigned the same probability of $1/(\text{nr. classes})$. The performance measure commonly used for this, e.g. by Ovadia et al. (2019), is to measure this through the discrete entropy of the class prediction outputs $H(Y|X_{\text{OoD}})$, which should be as high as possible.

OoD detection score: For OoD detection, we use the (unconditional) negative log-likelihood (NLL) predicted by each model as an outlier score. This is a basic approach, but also the most common in the generative classifier literature. For the VIB, the situation is different: as opposed to a VAE, it does not estimate $p(X)$ due to the missing reconstruction loss. As a substitute, we use the ELBO loss (also termed 'info-loss' in the VIB literature), that stems from the $I(X, Z)$ -term. Note, in the original VIB work, no OoD detection was performed, and this approach is not standard practice, so we only list these results for completeness.

To quantify the OoD detection capabilities of each model, we record the degree of separability between in-distribution data and OoD data: for a random inlier and a random outlier, what is the probability that the outlier has the higher outlier score. The detection score would be 1.0 for perfectly separated in- and outliers, and 0.5 if each point is assigned a random score. Note, this definition is exactly equal to the widely used ROC-AUC metric.

OoD datasets: The inlier dataset consist of CIFAR10/100 images, i.e. 32×32 colour images showing 10/100 object classes. Additionally we created four different OoD datasets, that cover different aspects, see

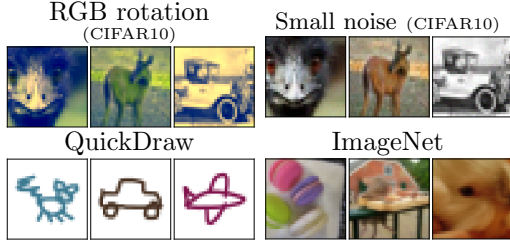


Figure 5: Examples from each OoD dataset used in the evaluation. The inlier data are original CIFAR10 images.

Fig. 5. Firstly, we create a random 3D rotation matrix with an adjustable rotation angle α , and apply it to the RGB color vectors of each pixel of CIFAR10 images. We set a fixed value of $\alpha = 0.3\pi$ for quantitative comparisons. Secondly, we add random uniform noise with a small amplitude to CIFAR10 images, as an alteration of the image statistics. Thirdly, we use the QuickDraw dataset of hand drawn objects (Ha & Eck, 2018), and filter only the categories corresponding to CIFAR10 classes and color each grayscale line drawing randomly. Therefore the semantic content is the same, but the image modality is different. Lastly, we downscale the ImageNet validation set to 32×32 pixels. In this case, the semantic content is different, but the image statistics are very similar to CIFAR10. However, we find that none of the models can reliably detect the ImageNet data as OoD, so we use this primarily to measure the prediction entropy behaviour on OoD data.

3.3 Quantitative Model Comparison

A comparison of all models is performed in Table 1 for CIFAR10 and CIFAR100. To our best knowledge, in the literature so far, generative classifiers have never been used for CIFAR100, as this is generally very challenging.

In summary, we find that the IB-INN has slightly worse classification performance than a standard DC, which is in line with the performance drop from feed-forward to invertible architecture (i-RevNet). However, the uncertainties in the form of calibration error and entropy on OoD data, are far superior. For ablation where only \mathcal{L}_Y is used ($\tilde{\beta} \rightarrow \infty$), the performance is more comparable to a standard DC, demonstrating that it is really the IB objective giving the improvements. In addition, the OoD detection is on par or better than for the other GCs. Furthermore, the GCs naively trained with class-NLL make no meaningful predictions on either dataset. While the regularized version achieves better accuracy, and maintains the OoD detection capabilities, the calibration and uncertainty is very poor. Lastly, we find that the VIB brings some improvement over a standard feed-forward model in terms of uncer-



Figure 6: Each column shows a latent space interpolation between two images (leftmost and rightmost). Each row corresponds to a model trained with a different $\tilde{\beta}$. We find that the generative performance decreases with higher $\tilde{\beta}$.

tainties, especially for CIFAR100, but still inferior to IB-INN.

3.4 Effect of Beta

To study the trade-off between classification performance and modeling capabilities parameterized by $\tilde{\beta}$, we train 24 IB-INN models for different $\tilde{\beta}$ ranging from 0.02 to 50. For comparison, we also train corresponding VIB models, and summarize our findings in Fig. 8. As expected, the classification accuracy improves as we increase $\tilde{\beta}$, while the uncertainty estimates become worse. The trend of OoD detection depends on the dataset: It is almost constant for the RGB rotated data, improves for the hand-drawn data, and degrades for the noisy data. This is due to whether the focus on class information is helpful in detecting OoD data, or whether simply modeling natural images suffices. The classification accuracy of the VIB stays almost constant over the whole range, and the uncertainties also show little variations, indicating that the used loss function is indeed only a rough bound on the true IB.

3.5 Latent Space Exploration

To better understand what the IB-INN learns, we analyze the latent space in different ways. Firstly, Fig. 7 shows the layout of the latent space GMM through a linear projection. We find that the clusters of ambiguous classes, e.g. truck and car, are connected in latent space, to account for uncertainty. Secondly, Fig. 6 shows interpolations in latent space between two test set images, using models trained with different values of $\tilde{\beta}$. We observe that for low $\tilde{\beta}$, the IB-INN has a very well structured latent space, resulting in good generative capabilities and plausible interpolations. For larger $\tilde{\beta}$, the interpolation quality continually degrades.

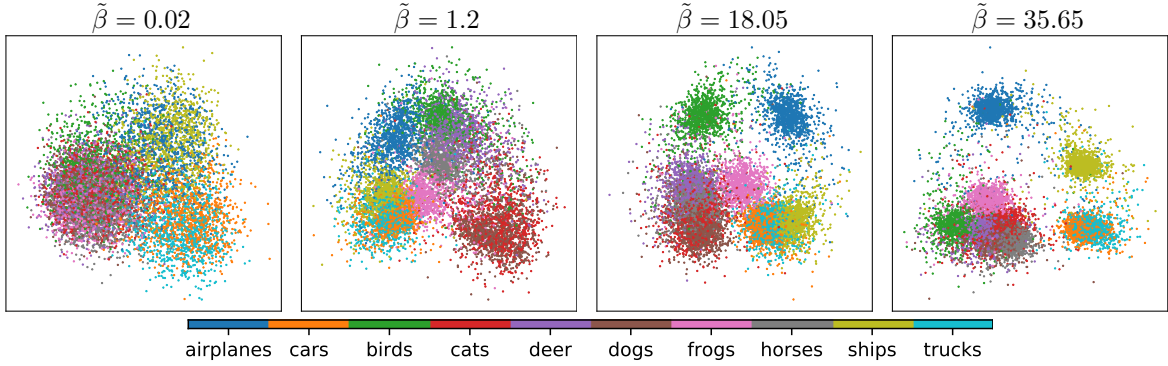


Figure 7: GMM Latent space behaviour by increasing $\tilde{\beta}$. The class separation increases with larger $\tilde{\beta}$. Note however, how ambiguous classes (truck and car) stay connected, to account for uncertainty.

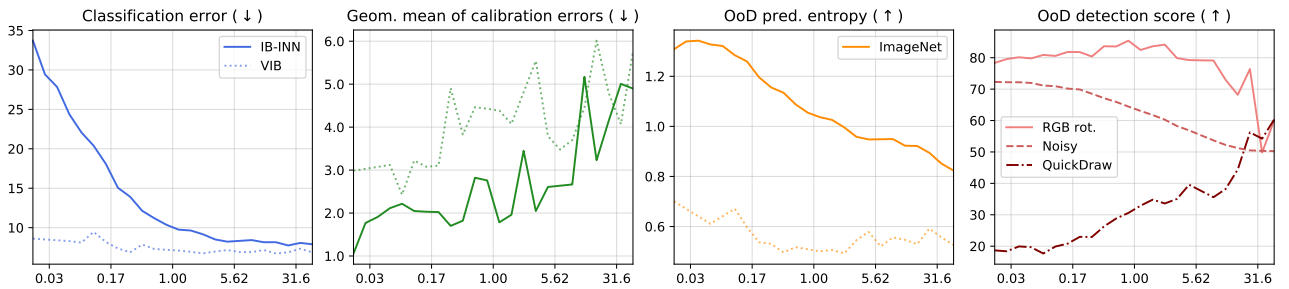


Figure 8: Effect of changing the parameter $\tilde{\beta}$ (logarithmic x -axis) on the different performance measures (y -axis). The VIB results are the dotted lines for comparison, except for OoD detection. The inlier dataset is CIFAR10. The arrows indicate if a larger or smaller score is better. While classification accuracy improves with $\tilde{\beta}$, the uncertainty measures grow worse. The trend for the OoD detection depends on the OoD data used, and whether the focus on class information is important for the detection. The special case $\beta = 1$ (class-NLL) translates to $\tilde{\beta} \approx 3 \cdot 10^{-4}$, where the classification accuracy is unusable (cf. Table 1). All curves shown separately in the appendix.

Table 1: Results on the CIFAR10 and CIFAR100 datasets. All models have the same number of parameters and were trained with the same hyperparameters. All values except entropy and overconfidence are given in percent. The arrows indicate whether a higher or lower value is better. The prediction entropy of the model trained with standard class-NLL is not taken into account, because the entropy is equally high on in-distribution data due to the poor classification performance. The OoD detection score for VIB is also not taken into account, see text.

CIFAR10	Classif.	Calibration error (\downarrow)				OoD prediction entropy (\uparrow)					OoD detection score (\uparrow)				
	err. (\downarrow)	Geo. mean	Expec.	Max	Overc.	Geo. mean	RGB-rot	Draw	Noise	ImgNet	Geo. mean	RGB-rot	Draw	Noise	ImgNet
IB-INN (ours, $\beta = 1$)	9.88	1.969	0.93	8.20	0.00	0.865	0.86	1.07	0.59	1.02	54.03	86.5	21.3	86.3	53.6
IB-INN, only \mathcal{L}_Y ($\tilde{\beta} \rightarrow \infty$)	8.29	6.690	1.22	23.81	10.32	0.587	0.55	0.68	0.43	0.74	58.72	59.7	96.4	50.9	40.6
IB-INN, only \mathcal{L}_X ($\tilde{\beta} = 0$)	–	–	–	–	–	–	–	–	–	–	44.68	79.3	12.1	80.4	51.9
Class-NLL	84.98	62.016	11.21	86.16	247.00	(1.067)	(1.03)	1.22	0.97	1.06)	48.55	80.2	18.6	71.6	52.0
Class-NLL (regularized)	20.57	24.176	3.93	20.30	177.33	0.002	0.00	0.00	0.00	0.00	48.95	82.0	16.1	79.1	54.9
VIB ($\beta = 1$)	7.29	4.466	0.68	27.83	4.71	0.342	0.35	0.38	0.19	0.52	(47.38)	(46.4)	52.2	50.0	(41.7)
Standard ResNet	6.76	5.656	0.73	40.61	6.12	0.344	0.35	0.44	0.18	0.51	–	–	–	–	–
i-RevNet	9.09	2.224	0.54	14.78	1.37	0.611	0.74	0.90	0.25	0.82	–	–	–	–	–

CIFAR100	Classif.	Calibration error (\downarrow)				OoD prediction entropy (\uparrow)					OoD detection score (\uparrow)				
	err. (\downarrow)	Geo. mean	Expec.	Max	Overc.	Geo. mean	RGB-rot	Draw	Noise	ImgNet	Geo. mean	RGB-rot	Draw	Noise	ImgNet
IB-INN (ours, $\beta = 1$)	36.59	1.157	0.15	6.67	1.54	2.314	2.58	2.43	2.11	2.17	51.21	79.1	27.9	61.7	50.6
IB-INN, only \mathcal{L}_Y ($\tilde{\beta} \rightarrow \infty$)	33.86	1.171	0.15	4.68	2.34	2.394	2.53	2.62	2.17	2.29	60.92	68.6	99.3	49.5	40.8
IB-INN, only \mathcal{L}_X ($\tilde{\beta} = 0$)	–	–	–	–	–	–	–	–	–	–	39.67	74.2	8.5	77.9	50.3
Class-NLL	98.59	34.452	1.47	92.86	298.65	(1.982)	(1.89)	2.37	1.75	1.97)	41.52	75.6	10.0	78.2	50.4
Class-NLL (regularized)	79.08	32.392	1.40	94.58	257.30	0.025	0.02	0.01	0.06	0.05	41.96	73.6	10.4	78.7	51.3
VIB ($\beta = 1$)	42.92	1.259	0.18	8.63	1.26	1.960	2.20	1.61	1.97	2.11	(48.00)	(43.0)	56.8	46.1	(47.1)
Standard ResNet	29.14	4.863	0.23	17.26	29.03	2.012	2.21	2.16	1.78	1.92	–	–	–	–	–
i-RevNet	34.27	2.880	0.24	17.76	5.50	1.762	2.16	1.71	1.55	1.69	–	–	–	–	–

4 RELATED WORK

Generative Classification: An in-depth analysis of the trade-offs between discriminative and generative models was first performed by Ng & Jordan (2001) and was later extended by Bouchard & Triggs (2004); Bishop & Lasserre (2007); Xue & Titterton (2010), who investigated the possibility of balancing the strengths of both methods via a hyperparameter. Promising applications of these ideas to natural language processing, based on neural networks, were recently presented by Shen et al. (2017); Yogatama et al. (2017); Wang & Wu (2018). Li et al. (2019) showed that generative classifiers may be more robust against adversarial attacks, and Hwang et al. (2019) demonstrated their robustness against missing data. On the other hand, Fetaya et al. (2019) found that conditional normalizing flows have poor discriminative performance, making them unsuitable for classification tasks.

Information Bottleneck: The IB was introduced by Tishby et al. (2000) as a tool for information-theoretic optimization of compression methods. This idea was expanded on by Chechik et al. (2005); Gilad-Bachrach et al. (2003); Shamir et al. (2010) and Friedman et al. (2013). A relationship between IB and deep learning was first proposed by Tishby & Zaslavsky (2015), and later experimentally examined by Shwartz-Ziv & Tishby (2017), who use IB for the understanding of neural network behavior and training dynamics. A close relation of IB to dropout, disentanglement, and variational autoencoding was discovered by Achille & Soatto (2018), which led them to introduce Information Dropout as a way to take advantage of IB in discriminative models. The approximation of IB in a variational setting was proposed independently by Kolchinsky et al. (2017) and Alemi et al. (2017), who especially demonstrate improved robustness against adversarial attacks.

5 CONCLUSIONS

We addressed the application of the Information Bottleneck (IB) to Invertible Neural Networks (INNs) as a loss function. We find that we can formulate an asymptotically exact version of the IB, which results in an INN that is a generative classifier. From our experiments, we conclude that the IB-INN provides higher quality uncertainties and out-of-distribution detection, while reaching almost the same classification accuracy as standard feed-forward methods, and generally outperforms other supervised generative classifiers on CIFAR10 and CIFAR100.

References

- Achille, A. and Soatto, S. Information dropout: Learning optimal representations through noisy computation. *IEEE Trans. Pattern Anal. Mach. Intell.*, 40(12):2897–2905, 2018. doi: 10.1109/TPAMI.2017.2784440. URL <https://doi.org/10.1109/TPAMI.2017.2784440>.
- Alemi, A. A., Fischer, I., Dillon, J. V., and Murphy, K. Deep variational information bottleneck. In *5th International Conference on Learning Representations, ICLR 2017, Toulon, France, April 24-26, 2017, Conference Track Proceedings*, 2017. URL <https://openreview.net/forum?id=HyxQzBceg>.
- Amjad, R. A. and Geiger, B. C. How (not) to train your neural network using the information bottleneck principle. *arXiv preprint arXiv:1802.09766*, 2018.
- Ardizzone, L., Lüth, C., Kruse, J., Rother, C., and Köthe, U. Guided image generation with conditional invertible neural networks. *CoRR*, abs/1907.02392, 2019. URL <http://arxiv.org/abs/1907.02392>.
- Belghazi, I., Rajeswar, S., Baratin, A., Hjelm, R. D., and Courville, A. C. MINE: mutual information neural estimation. *CoRR*, abs/1801.04062, 2018. URL <http://arxiv.org/abs/1801.04062>.
- Bishop, C. and Lasserre, J. Generative or discriminative? getting the best of both worlds. *Bayesian Statistics*, 8, January 2007. URL <https://www.microsoft.com/en-us/research/publication/generative-discriminative-getting-best-worlds/>.
- Bishop, C. M. *Pattern recognition and machine learning, 5th Edition*. Information science and statistics. Springer, 2007. ISBN 9780387310732.
- Bogachev, V. I., Kolesnikov, A. V., and Medvedev, K. V. Triangular transformations of measures. *Sbornik: Mathematics*, 196(3):309, 2005.
- Bouchard, G. and Triggs, B. The tradeoff between generative and discriminative classifiers. In *16th IASC International Symposium on Computational Statistics (COMPSTAT'04)*, pp. 721–728, 2004.
- Chechik, G., Globerson, A., Tishby, N., and Weiss, Y. Information bottleneck for gaussian variables. *J. Mach. Learn. Res.*, 6:165–188, 2005. URL <http://jmlr.org/papers/v6/chechik05a.html>.
- Cover, T. M. and Thomas, J. A. *Elements of information theory*. John Wiley & Sons, 2012.
- De Bruijn, N. G. *Asymptotic methods in analysis*, volume 4. Courier Corporation, 1981.

- Dinh, L., Sohl-Dickstein, J., and Bengio, S. Density estimation using real NVP. In *5th International Conference on Learning Representations, ICLR 2017, Toulon, France, April 24-26, 2017, Conference Track Proceedings*, 2017. URL <https://openreview.net/forum?id=HkpbH91x>.
- Fetaya, E., Jacobsen, J., and Zemel, R. S. Conditional generative models are not robust. *CoRR*, abs/1906.01171, 2019. URL <http://arxiv.org/abs/1906.01171>.
- Friedman, N., Mosenzon, O., Slonim, N., and Tishby, N. Multivariate information bottleneck. *CoRR*, abs/1301.2270, 2013. URL <http://arxiv.org/abs/1301.2270>.
- Gilad-Bachrach, R., Navot, A., and Tishby, N. An information theoretic tradeoff between complexity and accuracy. In *Computational Learning Theory and Kernel Machines, 16th Annual Conference on Computational Learning Theory and 7th Kernel Workshop, COLT/Kernel 2003, Washington, DC, USA, August 24-27, 2003, Proceedings*, pp. 595–609, 2003. doi: 10.1007/978-3-540-45167-9_43. URL https://doi.org/10.1007/978-3-540-45167-9_43.
- Guo, C., Pleiss, G., Sun, Y., and Weinberger, K. Q. On calibration of modern neural networks. In *Proceedings of the 34th International Conference on Machine Learning, ICML 2017, Sydney, NSW, Australia, 6-11 August 2017*, pp. 1321–1330, 2017. URL <http://proceedings.mlr.press/v70/guo17a.html>.
- Ha, D. and Eck, D. A neural representation of sketch drawings. In *6th International Conference on Learning Representations, ICLR 2018, Vancouver, BC, Canada, April 30 - May 3, 2018, Conference Track Proceedings*, 2018. URL <https://openreview.net/forum?id=Hy6GHpkCW>.
- He, K., Zhang, X., Ren, S., and Sun, J. Deep residual learning for image recognition. In *2016 IEEE Conference on Computer Vision and Pattern Recognition, CVPR 2016, Las Vegas, NV, USA, June 27-30, 2016*, pp. 770–778, 2016. doi: 10.1109/CVPR.2016.90. URL <https://doi.org/10.1109/CVPR.2016.90>.
- Huang, C.-W., Krueger, D., Lacoste, A., and Courville, A. Neural autoregressive flows. *arXiv preprint arXiv:1804.00779*, 2018.
- Hwang, U., Jung, D., and Yoon, S. Hexagan: Generative adversarial nets for real world classification. In *Proceedings of the 36th International Conference on Machine Learning, ICML 2019, 9-15 June 2019, Long Beach, California, USA*, pp. 2921–2930, 2019. URL <http://proceedings.mlr.press/v97/hwang19a.html>.
- Hyvärinen, A. and Pajunen, P. Nonlinear independent component analysis: Existence and uniqueness results. *Neural Networks*, 12(3):429–439, 1999.
- Jacobsen, J., Smeulders, A. W. M., and Oyallon, E. i-revnet: Deep invertible networks. In *6th International Conference on Learning Representations, ICLR 2018, Vancouver, BC, Canada, April 30 - May 3, 2018, Conference Track Proceedings*, 2018. URL <https://openreview.net/forum?id=HJsJkMb0Z>.
- Jacobsen, J., Behrmann, J., Zemel, R. S., and Bethge, M. Excessive invariance causes adversarial vulnerability. In *7th International Conference on Learning Representations, ICLR 2019, New Orleans, LA, USA, May 6-9, 2019*, 2019. URL <https://openreview.net/forum?id=BkfbpsAcF7>.
- Jaini, P., Selby, K. A., and Yu, Y. Sum-of-squares polynomial flow. *arXiv preprint arXiv:1905.02325*, 2019.
- Kingma, D. P. and Dhariwal, P. Glow: Generative flow with invertible 1x1 convolutions. In *Advances in Neural Information Processing Systems 31: Annual Conference on Neural Information Processing Systems 2018, NeurIPS 2018, 3-8 December 2018, Montréal, Canada*, pp. 10236–10245, 2018. URL <http://papers.nips.cc/paper/8224-glow-generative-flow-with-invertible-1x1-convolutions>.
- Kolchinsky, A., Tracey, B. D., and Wolpert, D. H. Nonlinear information bottleneck. *CoRR*, abs/1705.02436, 2017. URL <http://arxiv.org/abs/1705.02436>.
- L’Ecuyer, P. Note: On the interchange of derivative and expectation for likelihood ratio derivative estimators. *Management Science*, 41(4):738–747, 1995.
- Li, Y., Bradshaw, J., and Sharma, Y. Are generative classifiers more robust to adversarial attacks? In *Proceedings of the 36th International Conference on Machine Learning, ICML 2019, 9-15 June 2019, Long Beach, California, USA*, pp. 3804–3814, 2019. URL <http://proceedings.mlr.press/v97/li19a.html>.
- Nalisnick, E. T., Matsukawa, A., Teh, Y. W., Görür, D., and Lakshminarayanan, B. Hybrid models with deep and invertible features. In *Proceedings of the 36th International Conference on Machine Learning, ICML 2019, 9-15 June 2019, Long Beach, California, USA*, pp. 4723–4732, 2019a. URL <http://proceedings.mlr.press/v97/nalisnick19b.html>.
- Nalisnick, E. T., Matsukawa, A., Teh, Y. W., Görür, D., and Lakshminarayanan, B. Do deep generative

- models know what they don't know? In *7th International Conference on Learning Representations, ICLR 2019, New Orleans, LA, USA, May 6-9, 2019*, 2019b. URL <https://openreview.net/forum?id=H1xwNhCcYm>.
- Newey, W. K. and McFadden, D. Large sample estimation and hypothesis testing. *Handbook of econometrics*, 4:2111–2245, 1994.
- Ng, A. Y. and Jordan, M. I. On discriminative vs. generative classifiers: A comparison of logistic regression and naive bayes. In *Advances in Neural Information Processing Systems 14 [Neural Information Processing Systems: Natural and Synthetic, NIPS 2001, December 3-8, 2001, Vancouver, British Columbia, Canada]*, pp. 841–848, 2001. URL <http://papers.nips.cc/paper/2020-on-discriminative-vs-generative-classifiers-a-comparison-of-logistic-regression-and-naive-bayes>.
- Ovadia, Y., Fertig, E., Ren, J., Nado, Z., Sculley, D., Nowozin, S., Dillon, J. V., Lakshminarayanan, B., and Snoek, J. Can you trust your model's uncertainty? evaluating predictive uncertainty under dataset shift. *CoRR*, abs/1906.02530, 2019. URL <http://arxiv.org/abs/1906.02530>.
- Serfling, R. J. *Approximation theorems of mathematical statistics*, volume 162. John Wiley & Sons, 2009.
- Shamir, O., Sabato, S., and Tishby, N. Learning and generalization with the information bottleneck. *Theor. Comput. Sci.*, 411(29-30):2696–2711, 2010. doi: 10.1016/j.tcs.2010.04.006. URL <https://doi.org/10.1016/j.tcs.2010.04.006>.
- Shen, P., Lu, X., Li, S., and Kawai, H. Conditional generative adversarial nets classifier for spoken language identification. In *Interspeech 2017, 18th Annual Conference of the International Speech Communication Association, Stockholm, Sweden, August 20-24, 2017*, pp. 2814–2818, 2017. URL http://www.isca-speech.org/archive/Interspeech_2017/abstracts/0553.html.
- Shwartz-Ziv, R. and Tishby, N. Opening the black box of deep neural networks via information. *CoRR*, abs/1703.00810, 2017. URL <http://arxiv.org/abs/1703.00810>.
- Szegedy, C., Vanhoucke, V., Ioffe, S., Shlens, J., and Wojna, Z. Rethinking the inception architecture for computer vision. In *2016 IEEE Conference on Computer Vision and Pattern Recognition, CVPR 2016, Las Vegas, NV, USA, June 27-30, 2016*, pp. 2818–2826, 2016. doi: 10.1109/CVPR.2016.308. URL <https://doi.org/10.1109/CVPR.2016.308>.
- Tishby, N. and Zaslavsky, N. Deep learning and the information bottleneck principle. In *2015 IEEE Information Theory Workshop, ITW 2015, Jerusalem, Israel, April 26 - May 1, 2015*, pp. 1–5, 2015. doi: 10.1109/ITW.2015.7133169. URL <https://doi.org/10.1109/ITW.2015.7133169>.
- Tishby, N., Pereira, F. C. N., and Bialek, W. The information bottleneck method. *CoRR*, physics/0004057, 2000. URL <http://arxiv.org/abs/physics/0004057>.
- Wang, Z. and Wu, Q. An integrated deep generative model for text classification and generation. *Mathematical Problems in Engineering*, 2018, 2018.
- Xue, J. and Titterton, D. M. On the generative-discriminative tradeoff approach: Interpretation, asymptotic efficiency and classification performance. *Computational Statistics & Data Analysis*, 54(2):438–451, 2010. doi: 10.1016/j.csda.2009.09.011. URL <https://doi.org/10.1016/j.csda.2009.09.011>.
- Yogatama, D., Dyer, C., Ling, W., and Blunsom, P. Generative and discriminative text classification with recurrent neural networks. *CoRR*, abs/1703.01898, 2017. URL <http://arxiv.org/abs/1703.01898>.

Exact Information Bottleneck with Invertible Neural Networks: Getting the Best of Discriminative and Generative Modeling

– Appendix –

6 PROOFS AND DERIVATIONS

6.1 Mutual Cross-Information as Estimator for MI

In our case, we only require $CI(X, Z_\mathcal{E})$ and $CI(Y, Z_\mathcal{E})$, but we show the correspondence for two unspecified random variables U, V , as it may be of general interest. However, note that our estimator will likely not be particularly useful outside of our specific use-case, and other methods should be preferred (e.g. Belghazi et al., 2018).

For the joint input space $\Omega = \mathcal{U} \times \mathcal{V}$, we assume that \mathcal{U} is a compact domain in \mathbb{R}^d , and \mathcal{V} is either also a compact domain in \mathbb{R}^l (Case 1), or discrete, i.e. a finite subset of \mathbb{N} (Case 2). In Case 1, we assume that $p(U, V)$ is absolutely continuous with respect to the Lebesgue measure, and in Case 2, $p(U|v)$ is absolutely continuous for all values of $v \in \mathcal{V}$.

In Case 1, $q(U)$, $q(V)$, $q(U, V)$, the densities can all be modeled separately, by three flow networks $g_\theta^{(U)}(u)$, $g_\theta^{(V)}(v)$, $g_\theta^{(UV)}(u, v)$. Although in our formulation, we are later able to approximate the latter two through the first.

In Case 2, we only model $q(U|V)$, and assume that $q(V)$ is either known beforehand and set to $p(V)$ (e.g. label distribution), or the probabilities are parametrized directly. Either way, $q(U, V) = q(U|V)q(V)$ and $q(U) = \sum_{v \in \mathcal{V}} q(U, v)$.

Proposition 1. *Assume that the $q(\cdot)$ densities can be chosen from a sufficiently rich model family (e.g. a universal density estimator). Then for every $\eta > 0$ there is a model such that*

$$|I(U, V) - CI(U, V)| < \eta \quad (15)$$

and $I(U, V) = CI(U, V)$ if $p(U, V) = q(U, V)$.

Proof. Writing out the definitions explicitly, and rearranging, we find

$$\begin{aligned} CI(U, V) &= I(U, V) + D_{\text{KL}}(p(U, V) \| q(U, V)) \\ &\quad - D_{\text{KL}}(p(U) \| q(U)) - D_{\text{KL}}(p(V) \| q(V)) \end{aligned} \quad (16)$$

Shortening the KL terms to D_1 , D_2 and D_3 for convenience:

$$|I_{\theta^*}(U, V) - I(U, V)| = |D_1 - D_2 - D_3| \quad (17)$$

$$\leq D_1 + D_2 + D_3 \quad (18)$$

$$\leq 3 \max(D_1, D_2, D_3) \quad (19)$$

At this point, we can simply apply results from measure transport: if the g_θ are from a family of universal density estimators, we can choose θ^* to make $\max(D_1, D_2, D_3)$ arbitrarily small by matching p and q . This was shown in general for increasing triangular maps, e.g. in Hyvärinen & Pajunen (1999), Theorem 1 for an accessible proof, or Bogachev et al. (2005) for a more in-depth approach (specifically Corollary 4.2). Generality was also proven for several concrete architectures, e.g. Jaini et al. (2019), Huang et al. (2018).

For the second part of the Proposition, we note the following: if $p(U, V) = q(U, V)$, we have $D_1 = D_2 = D_3 = 0$, and therefore $CI(U, V) = I(U, V)$. \square

6.2 Loss Function \mathcal{L}_X

In the following, we use the subscript-notation for the cross entropy:

$$h_q(U) = \mathbb{E}_{u \sim p(U)} [-\log q(u)], \quad (20)$$

to avoid confusion with the joint entropy that arises with the usual notation ($h(p(U), q(U))$).

We use an INN g_θ representing a homeomorphic transform, where the network parameter space Θ is a compact subdomain of \mathbb{R}^n . We assume that $g_\theta(u)$ and J_θ are uniformly bounded, and furthermore the absolute Jacobian determinant $|\det J_\theta|$ is also uniformly bounded from below by a constant > 0 . We also assume J_θ is continuous and differentiable in both X and θ . All these assumptions are fulfilled for most architectures used in practice, and certainly for the coupling block design. As J_θ is bounded, this also implies that g_θ is Lipschitz-continuous. The X input space \mathcal{X} is a compact subdomain of \mathbb{R}^d .

Proposition 2. *For the case given in the paper, that $Z_\mathcal{E} = g_\theta(X + \mathcal{E})$, it holds that $I(X, Z_\mathcal{E}) \leq CI(X, Z_\mathcal{E})$.*

Proof. In the following, we first use the invariance of the (cross-)information to homeomorphic transforms.

Then, we use $p(X+\mathcal{E}|X) = q(X+\mathcal{E}|X) = p(\mathcal{E})$ (known exactly) and write out all the terms, most of which cancel. Finally, we use the inequality that the cross entropy is larger than the entropy, $h_q(U) \geq h(U)$ regardless of q . The equality holds iff the two distributions are the same.

$$CI(X, Z_\mathcal{E}) - I(X, Z_\mathcal{E}) = CI(X, X+\mathcal{E}) - I(X, X+\mathcal{E}) \quad (21)$$

$$= h_q(X) - h(X) + 0 \quad (22)$$

$$\geq 0 \quad (23)$$

With equality iff $p(X) = q(X)$. \square

We now want to show that the network optimization procedure that arises from the empirical loss, in particular the gradients w.r.t. network parameters θ , are consistent with those of $CI(X, Z_\mathcal{E})$:

Proposition 3. *The defined loss is a consistent estimator for $CI(X, Z_\mathcal{E})$ up to a known constant, and a consistent estimator for the gradients. Specifically, for any $\epsilon_1, \epsilon_2 > 0$ and $0 < \delta < 1$ there are $\sigma_0 > 0$ and $N_0 \in \mathbb{N}$, such that $\forall N \geq N_0$ and $\forall \sigma < \sigma_0$,*

$$\Pr\left(\left|CI(X, Z_\mathcal{E}) + d \log \sqrt{2\pi e \sigma^2} - \mathcal{L}_X^{(N)}\right| < \epsilon_1\right) > 1 - \delta$$

and

$$\Pr\left(\left\|\frac{\partial}{\partial \theta} CI(X, Z_\mathcal{E}) - \frac{\partial}{\partial \theta} \mathcal{L}_X^{(N)}\right\| < \epsilon_2\right) > 1 - \delta$$

holds uniformly for all model parameters θ .

The loss function is as defined in the paper:

$$\mathcal{L}_X = h_q(Z_\mathcal{E}) - \mathbb{E}_{x \sim p(X+\mathcal{E})} \left[\log |\det J_\theta(x)| \right] \quad (24)$$

as well as its empirical estimate using N samples, $\mathcal{L}_X^{(N)}$.

We split the proof into two Lemmas, which we will later combine.

Lemma 1. *For any $\eta_1, \eta_2 > 0$ and $\delta > 0$ there is an $N_0 \in \mathbb{N}$ so that*

$$\Pr\left(|\mathcal{L}_X^{(N)} - \mathcal{L}_X| < \eta_1\right) > 1 - \delta \quad (25)$$

$$\Pr\left(\left|\frac{\partial}{\partial \theta} \mathcal{L}_X^{(N)} - \frac{\partial}{\partial \theta} \mathcal{L}_X\right| < \eta_2\right) > 1 - \delta \quad (26)$$

$$\forall N \geq N_0$$

Proof. For the first part (Eq. 25), we simply have to show that the uniform law of large numbers applies, specifically that all expressions in the expectations are bounded and change continuously with θ . For the Jacobian term in the loss, this is the case by definition. For the $h_q(Z_\mathcal{E})$ -term, we can show the boundedness

of $\log q$ occurring in the expectation by inserting the GMM explicitly. We find

$$-\log(q(z)) \leq \max_y [(z - \mu_y)^2 / 2] + \text{const.} \quad (27)$$

while we know that $z = g_\theta(x)$ is bounded. Therefore, the uniform law of large numbers (Newey & McFadden, 1994, Lemma 2.4) guarantees existence of an N_1 to satisfy the condition for all $\theta \in \Theta$.

For the second part (Eq. 26), we will show that the gradient w.r.t. θ and the expectation can be exchanged, as the gradient is also bounded by the same arguments as before. We find that the conditions for exchanging expectation and gradient are trivially satisfied, again due to the bounded gradients (see L'Ecuyer (1995), assumption A1, with Γ set to the upper bound). This results in an $N_2 \in \mathbb{N}$ for which Eq. 26 is satisfied. As a last step, we simply define $N_0 := \max(N_1, N_2)$. \square

Lemma 2. *For any $\eta_1, \eta_2 > 0$ there is an $\sigma_0 > 0$, so that*

$$\left\|CI_\theta(X, Z_\mathcal{E}) + d \log \sqrt{2\pi e \sigma^2} - \mathcal{L}_X\right\| < \eta_2 \quad (28)$$

$$\left\|\frac{\partial}{\partial \theta} (CI_\theta(X, Z_\mathcal{E}) - \mathcal{L}_X)\right\| < \eta_2 \quad (29)$$

$$\forall \sigma < \sigma_0$$

Proof. In the following proof, we make use of the $O(\cdot)$ notation, see e.g. De Bruijn (1981):

We write $f(\sigma) = O(g(\sigma))$ ($\sigma \rightarrow 0$) iff there exists a σ_0 and an $M \in \mathbb{R}$, $M > 0$ so that

$$\|f(\sigma)\| < M g(\sigma) \quad \forall \sigma \leq \sigma_0. \quad (30)$$

Furthermore, to discuss the limit case, it is necessary we reparametrize the noise variable \mathcal{E} in terms of noise S with a fixed standard normal distribution:

$$\mathcal{E} = \sigma S \quad \text{with} \quad p(S) = \mathcal{N}(0, 1) \quad (31)$$

To begin with, we use the invariance of CI under the homeomorphic transform g_θ . This can be easily verified by inserting the change-of-variables formula into the definition. See e.g. Cover & Thomas (2012) Sec. 8.6. This results in

$$CI(X, Z_\mathcal{E}) = CI(Z, Z_\mathcal{E}) = h_q(Z_\mathcal{E}) - h_q(Z_\mathcal{E}|Z) \quad (32)$$

Next, we series expand $Z_\mathcal{E}$ around $\sigma = 0$. We can use Taylor's theorem to write

$$Z_\mathcal{E} = Z + J_\theta(Z)\mathcal{E} + O(\sigma^2) \quad (33)$$

We have written the Jacobian dependent on Z , but note that it is still $\partial g_\theta / \partial X$, and we simply substituted

the argument. We put this into the second entropy term $h_q(Z_{\mathcal{E}}|Z)$ in Eq. 32, and then perform a zero-order von Mises expansion of h_q . In general, the identity is

$$h_q(W + \xi) = h_q(W) + O(\|\xi\|) \quad (\|\xi\| \rightarrow 0), \quad (34)$$

and we simply put $\xi = O(\sigma^2)$ (the identity applies in the same way to the *conditional* cross-entropy). Intuitively, this is what we would expect: the entropy of an RV with a small perturbation should be approximately the same without the perturbation. See e.g. Serfling (2009), Sec. 6 for details. Effectively, this allows us to write the residual outside the entropy:

$$h_q(Z_{\mathcal{E}}|Z) = h_q(Z + J_{\theta}(Z)\mathcal{E} + O(\sigma^2)|Z) \quad (35)$$

$$= h_q(Z + J_{\theta}(Z)\mathcal{E}|Z) + O(\sigma^2) \quad (36)$$

$$= h_q(J_{\theta}(Z)\mathcal{E}|Z) + O(\sigma^2) \quad (37)$$

At this point, note that $q_{\theta}(J_{\theta}(Z)\mathcal{E}|Z)$ is simply a multivariate normal distribution, due to the conditioning on Z . In this case, we can use the entropy of a multivariate normal distribution, and simplify to obtain the following:

$$-h_q(J_{\theta}\mathcal{E}|Z) = \mathbb{E} \left[\frac{1}{2} \log (\det(2\pi\sigma^2 J_{\theta} J_{\theta}^T)) \right] \quad (38)$$

$$= \mathbb{E} \left[\frac{1}{2} \log ((2\pi\sigma^2)^d \det(J_{\theta})^2) \right] \quad (39)$$

$$= d \log \sqrt{2\pi e \sigma^2} + \mathbb{E} [\log |\det J_{\theta}|]. \quad (40)$$

Here, we exploited the fact that $J_{\theta}(Z)$ is an invertible matrix, and used $d = \dim(Z)$. Finally, as in practice we only want to evaluate the model once, we use the differentiability of J_{θ} to replace

$$\mathbb{E} [\log |\det J_{\theta}(Z)|] = \mathbb{E} [\log |\det J_{\theta}(Z_{\mathcal{E}})|] + O(\sigma). \quad (41)$$

The residual can be written outside of the expectation as we know it is bounded from our assumptions about g_{θ} and J_{θ} (Dominated Convergence theorem).

Putting the terms together, we obtain

$$CI(X, Z_{\mathcal{E}}) = h_q(Z_{\mathcal{E}}) - d \log \sqrt{2\pi e \sigma^2} - \mathbb{E} [\log |\det J_{\theta}|] + O(\sigma) \quad (42)$$

$$= \mathcal{L}_X - d \log \sqrt{2\pi e \sigma^2} + O(\sigma) \quad (43)$$

Through the definition of $O(\cdot)$, Eq. 28 is satisfied. To show that the gradients also agree (Eq. 29), we must ensure that the $O(\sigma)$ term is uniformly convergent to 0 over θ , i.e. there is a single constant M in the definition of $O(\cdot)$ that applies for all $\theta \in \Theta$. This is directly the case, as g_{θ} is Lipschitz continuous and the outputs are bounded (Arzela - Ascoli theorem). \square

We can now combine the two Lemmas 1 and 2, to show Proposition 3.

Proposition 3 - Proof.

Proof. The Proposition follows directly from Lemmas 1 and 2: for a given ϵ_1, ϵ_2 and δ , we choose each $\eta_i = \epsilon_i/2$, and apply the triangle inequality, meaning there exists an N_0 and σ_0 so that

$$\begin{aligned} & \left| CI(X, Z_{\mathcal{E}}) + d \log \sqrt{2\pi e \sigma^2} - \mathcal{L}_X^{(N)} \right| \\ & \leq \left| CI(X, Z_{\mathcal{E}}) + d \log \sqrt{2\pi e \sigma^2} - \mathcal{L}_X \right| + \left| \mathcal{L}_X - \mathcal{L}_X^{(N)} \right| \\ & < \frac{\epsilon_1}{2} + \frac{\epsilon_1}{2} \end{aligned}$$

And therefore $\Pr(\dots) > 1 - \delta$. Equivalently for the gradients. \square

7 NETWORK ARCHITECTURE

As in previous works, our INN architecture consists of so-called *coupling blocks*. In our case, each block consists of one affine coupling (Dinh et al., 2017), illustrated in Fig. 9, followed by random and fixed soft permutation of channels (Ardizzone et al., 2019), and a fixed scaling by a constant, similar to ActNorm layers introduced by Kingma & Dhariwal (2018). For the coupling coefficients, each subnetwork predicts multiplicative and additive components jointly, as done by Kingma & Dhariwal (2018). Furthermore, we adopt the soft clamping of multiplication coefficients used by Dinh et al. (2017).

For downsampling blocks, we introduce a new scheme, whereby we apply the i-RevNet downsampling (Jacobsen et al., 2018) only to the inputs to the affine transformation (u_2 branch in Fig. 9), while the affine coefficients are predicted from a higher resolution u_1 by using a strided convolution in the corresponding subnetwork. After this, i-RevNet downsampling is applied to the other half of the channels u_1 to produce v_1 , before concatenation and the soft permutation. We adopt this scheme as it more closely resembles the standard ResNet downsampling blocks, and makes the downsampling operation at least partly learnable.

We then stack sets of these blocks, with downsampling blocks in between, in the manner of [8, down, 25, down, 25]. Note, we use fewer blocks for the first resolution level, as the data only has three channels, limiting the expressive power of the blocks at this level. Finally, we apply a discrete cosine transform to replace the global average pooling in ResNets, as introduced by Jacobsen et al. (2019), followed by two blocks with fully connected subnetworks.

We perform training with SGD, learning rate 0.1, momentum 0.9, and batch size 128, as in the original

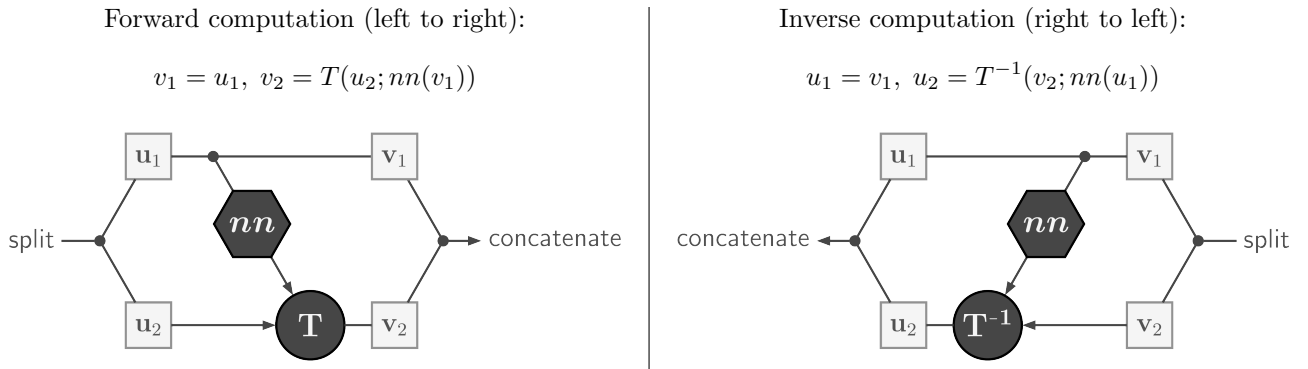


Figure 9: Illustration of a coupling block. T represents some invertible transformation, in our case an affine transformation. The transformation coefficients are predicted by a subnetwork (nn), which contains fully-connected or convolutional layers, nonlinear activations, batch normalization layers, etc., similar to the residual subnetwork in a ResNet (He et al., 2016). Note that the subnetwork does not have to be inverted itself.

ResNet publication by (He et al., 2016). We train for 450 epochs, decaying the learning rate by a factor of 10 after 150, 250, and 350 epochs.

8 ADDITIONAL EXPERIMENTS

In Figure 11 we show the trajectory of a sample in latent space, when gradually increasing the RGB-rotation OoD augmentation used in the paper. It travels from in-distribution to out-of-distribution. Note that such images were never seen during training.

Figure 10 provides all the performance metrics discussed in the paper over the range of $\tilde{\beta}$.

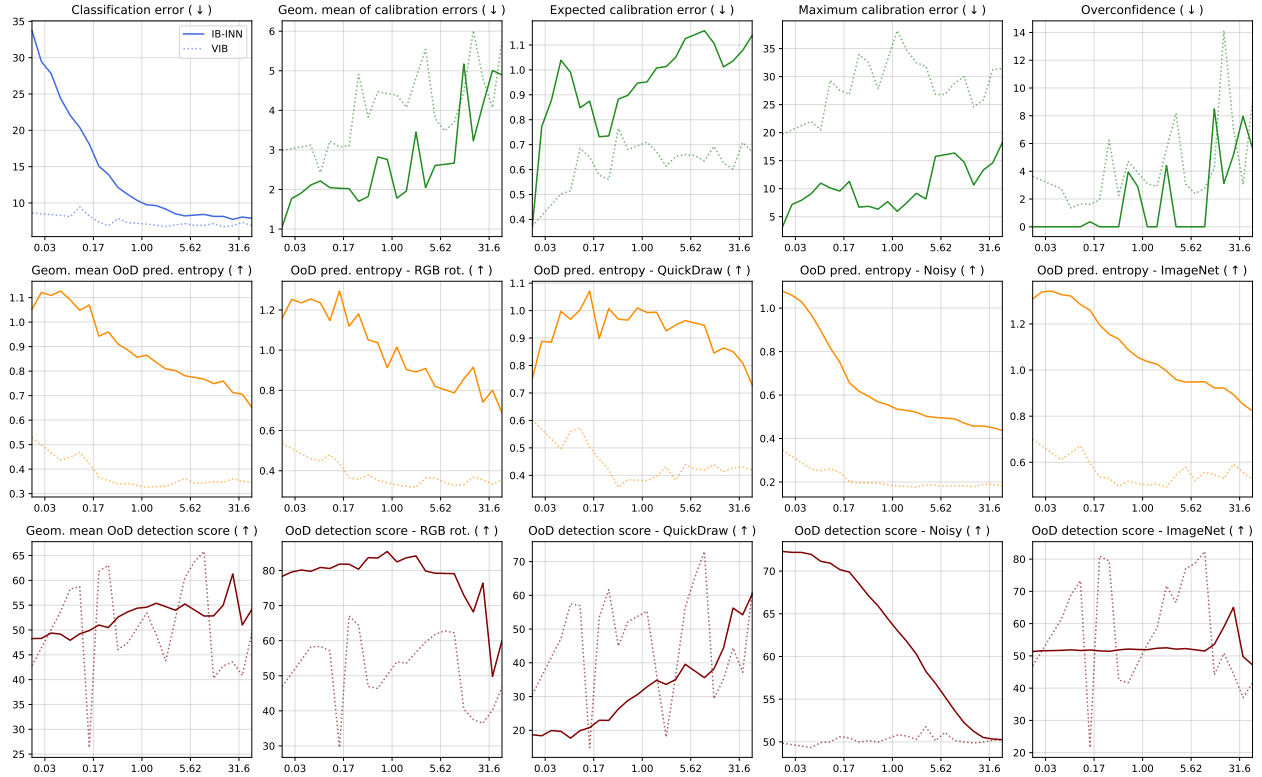


Figure 10: Effect of changing the parameter $\tilde{\beta}$ (x -axis) on the different performance measures (y -axis). The VIB results are added as dotted lines for comparison. The arrows indicate if a larger or smaller score is better. Details are explained in the paper.

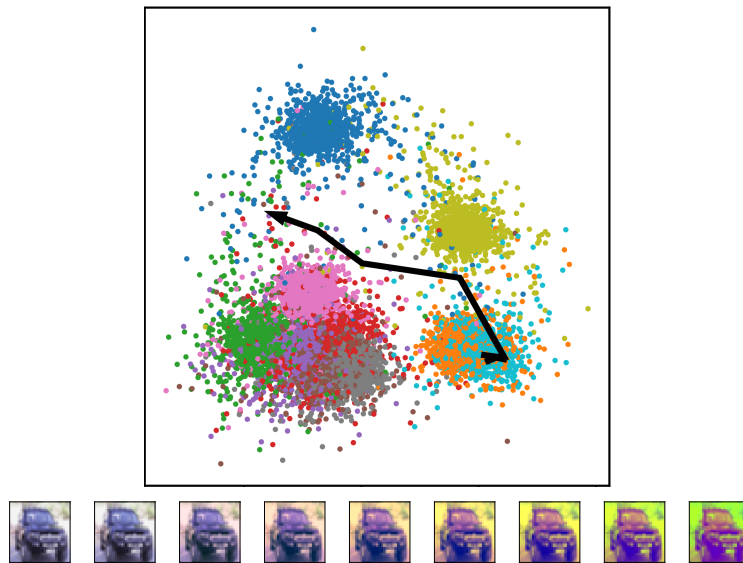


Figure 11: The scatter plot shows the location of test set data in latent space. A single sample is augmented by rotating the RGB color vector as described in the paper. The small images show the successive steps of augmentation, while the black arrow shows the position of each of these steps in latent space. We observe how the points in latent space travel further from the cluster center with increasing augmentation, causing them to be detected as OoD.